Structural Properties of Ionic Detergent Aggregates: A Large-Scale Molecular Dynamics Study of Sodium Dodecyl Sulfate

Maria Sammalkorpi,*,† Mikko Karttunen,‡ and Mikko Haataja†

Department of Mechanical and Aerospace Engineering, Princeton University, Princeton, NJ, and Department of Applied Mathematics, The University of Western Ontario, London, Ontario, Canada

Received: April 2, 2007; In Final Form: July 27, 2007

The properties of sodium dodecyl sulfate (SDS) aggregates were studied through extensive molecular dynamics simulations with explicit solvent. First, we provide a parametrization of the model within Gromacs. Then, we probe the kinetics of aggregation by starting from a random solution of SDS molecules and letting the system explore its kinetic pathway during the aggregation of multiple units. We observe a structural transition for the surfactant aggregates brought upon by a change in temperature. Specifically, at low temperatures, the surfactants form crystalline aggregates, whereas at elevated temperatures, they form micelles. We also investigate the dependence of aggregation kinetics on surfactant concentration and report on the molecular level structural changes involved in the transition.

1. Introduction

Self-assembly across length and time scales is a fundamental characteristic feature of all living systems. For example, protein folding processes, the formation of nucleosomes, and endo- and exocytosis are all critically dependent on self-assembly and -organization. It is, therefore, not surprising that much of the contemporary research in the pharmaceutical sciences, chemistry, and nanotechnology is driven by a quest to understand and control self-assembly from the fundamental as well as technological perspectives. Excellent overviews of the diverse systems and phenomena related to self-assembly can be found in refs 1−3.

Micelle formation is a generic feature of systems consisting of amphiphilic molecules (surfactants), proteins, peptides, and block-copolymers. In aqueous solutions at concentrations higher than their critical micellization concentration (CMC), surfactants form insoluble crystals (below their critical micellization temperature) or micelles (above the critical micellization temperature);[4,5] the surfactants can also form connected structures with complex and rich topologies, for example, in the case of block-copolymers.[6] Concentrated solutions typically give rise to more complex mesophases, such as the cubic phase or lamellar phase.[5,7] Due to their amphiphilic nature, surfactants aggregate at interfaces, and they can, for example, solubilize molecules that otherwise would not be soluble. An example of this is the detergent-mediated solvation of membrane proteins. Micelles have been employed, for example, in drug delivery in the so-called immunomicelles,[8] and micellar structures of amyloid protein assemblies have been suggested to play a important role in Alzheimer's disease.[9]

It is noteworthy that physically, the formation of new morphologies and spatial structures is typically associated with phase transitions and is accompanied by the subsequent emergence of new collective properties. In the case of micelle formation, however, there are no singularities in thermodynamic quantities, although finite-sized aggregates form spontaneously. Therefore, although micellization is not a thermodynamic phase transition, it is associated with the appearance of large (but finite) molecular aggregates.

From a computational perspective, direct simulations of self-assembly processes at the molecular level are very demanding. The reasons for this are two-fold. First, typical CMCs are on the order of $10^{-5}-10^{-3}$ M and aggregate sizes on the order of 100. Thus, a direct simulation with explicit solvent would require on the order of 10^7 solvent particles, which is prohibitively large. Second, micelle formation times are typically on the order of 10^{-4} s, which implies that extremely long simulations are required to probe the equilibrium behavior of these systems near CMC. For a review about simulations of surfactant solutions, please see Shelley and Shelley.[10]

Early computational micellization studies include lattice-based, coarse-grained models[11−15] as well as continuum simulations,[16,17] both of which have provided important insight into phase behavior of these systems. More recently, coarse grained[18−21] and atomistic studies with and without solvent have been carried out.[22−28] These simulations usually start from a spherical or rodlike micelle with a predetermined number of detergent molecules.[19,22,25,27,29] Although such an approach provides insight into detergent dynamics and micelle structure within that particular initial setup, the results implicitly contain the assumption that the global minimum energy configuration (that is, micellar shape and aggregation number) is close to the initial configuration. Interestingly, Marrink et al.[24] studied the dynamics of micellization of 54 dodecylphosphocholine (DPC) molecules starting from a random initial configuration and reported that the resulting aggregate structure depends on concentration. Lazaridis et al.[28] simulated 960 DPC molecules in an implicit environment, providing to date the temporally most extensive micellization data but without explicit solvent. Very recently, models that combine atomistic simulations and thermodynamics[30] have emerged.

In this paper, we focus on the formation of micellar structures from SDS surfactant solutions. Here, we are interested in self-

* To whom correspondence should be addressed. Formerly M. Huhtala.
† Princeton University.
‡ The University of Western Ontario.

10.1021/jp072587a CCC: $37.00
Published on Web 09/18/2007

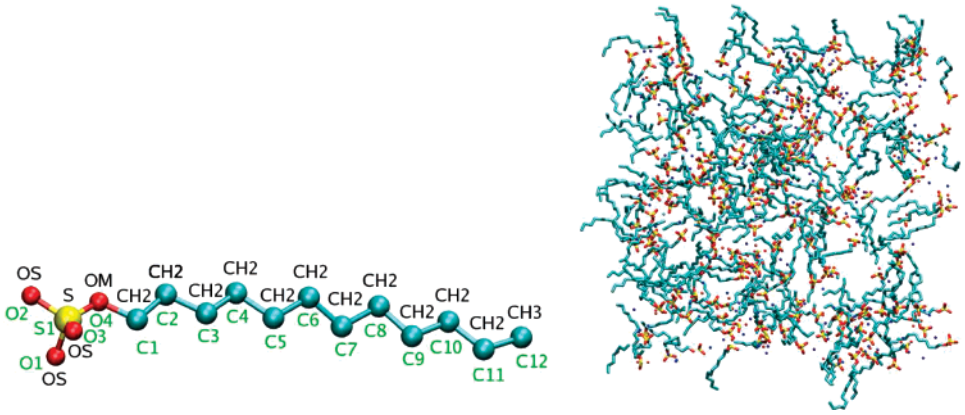

Figure 1. Left: The dodecyl sulfate molecule with the employed Gromacs atom types (black). The reference numbers of each atom (green) are also shown. Oxygen atoms O1−O3 are equivalent. Right: An example of a random initial configuration of the 1 M 200 SDS-molecule system. For clarity, the 7902 water molecules are omitted from the visualization.

assembly in thermodynamic equilibrium systems and the kinetic pathway to an equilibrium structure; in particular, no external driving forces are present. Specifically, we are interested in the formation kinetics of micelles via self-assembly. To our knowledge, this is the first systematic study in which micellization has been studied starting from a random initial configuration with a sufficient number of detergent molecules (200) to form multiple micelles at the atomistic level with explicit solvent. Our simulations are among the most extensive to-date (200 ns) and cover a wide temperature range (including the critical micellization temperature) to reveal the related structural changes in the aggregates.

The rest of this paper is organized as follows. The next section is devoted to the description of the model, its parameters, and computational details. Then, in Section 2.3, we summarize the analysis methods, after which the results are presented in Section 3. Herein, we first report on the equilibrium behavior of an isolated SDS molecule in solution, that is, the dilute limit. Subsequently we turn to a detailed analysis of the micellization process in a concentrated solution. In particular, we focus on the variations in micelle sizes and structures as a function of temperature and surfactant concentration. In this section, we also carefully assess the influence of finite system size on the results. Finally, we finish with a discussion of the results and conclusions in Section 5.

2. Methods

2.1. Computational Model. The Gromacs 3.3 simulation package[31−33] with the united atom parametrization was employed for the molecular dynamics (MD) simulations. The energies of the initial configurations were minimized with the steepest descent method. After the initialization, all simulations were performed in the NpT ensemble at $p = 1$ bar using the Berendsen barostat and thermostat[34] with coupling time constants of 1.0 ps and 0.1 ps, respectively. The temperatures of the solute, counterions, and solvent were controlled independently. The bond lengths of the detergent molecules were constrained by the LINCS algorithm,[35] and those of the water molecules, by SETTLE.[36] A time step of 2 fs was used throughout the simulations. The Lennard-Jones interactions were cut off at 1 nm, and the full particle-mesh Ewald method[37] was employed for the long-ranged electrostatic interactions; not fully accounting for these long-ranged electrostatic interactions has been shown to lead to serious artifacts in the simulation results.[38−40]

TABLE 1: Parameters for the SDS Molecule Covalent Bonds[41 a]

type i	type j	f	b_0 nm	k_b kJ mol^{-1} nm^{-2}	source
S	OM	1	0.150	376 650.0	
S	OS	1	0.136	376 560.0	C-OA
OS	CH2	1	0.143	251 040.0	
CH2	CH2	1	0.153	334 720.0	
CH3	CH2	1	0.153	334 720.0	

[a] The force constants are symmetric with respect to particle exchange: $i-j = j-i$.

TABLE 2: Parameters for the SDS Molecule Angles[41 a]

type i	type j	type k	f	ϕ_0 deg	k_ϕ kJ mol^{-1} rad^{-2}	source
OM	S	OM	1	109.5	520.00	
OS	S	OM	1	109.5	520.00	OM−S−OM
CH2	OS	S	1	120.0	397.50	approximated from existing parameters
CH2	CH2	OS	1	109.5	460.24	CH2−CH2−OM
CH2	CH2	CH2	1	111.0	460.24	
CH2	CH2	CH3	1	111.0	460.24	

[a] Parameters are symmetric: $i-j-k = k-j-i$.

TABLE 3: Parameters for the SDS Molecule Dihedral Angles[41 a]

type i	type j	type k	type l	f	ϕ deg.	k_ϕ kJ mol^{-1}	n	source
X	OS	S	X	1	0.0	3.766	3	C−OS (or SI−OS, or CH1-OS, or OS-CH2)
X	OS	CH2	X	1	0.0	3.766	3	C−OS (or SI−OS, or CH1-OS, or OS-CH2)
X	CH2	CH2	X	1	0.0	5.858	3	

[a] X stands for a nonspecified atom.

In its present implementation, the parameters for the SDS molecule have not been incorporated within Gromacs. We have chosen to employ existing Gromacs atom types, as depicted in Figure 1, and the existing force constants[41] as the basis of our SDS parametrization. The parameters are presented in Tables 1−4. The sodium ions were described by the Gromacs parameters. For a detailed analysis of different Na^+ parameters with different water models, please see ref 42. The simple point charge (SPC) water model[43] was adopted for the water molecules. Visualizations of all molecular configurations were generated with VMD.[44]

2.2. Simulated System. To characterize the model, we first studied the behavior of an isolated SDS molecule in solution at $T = 323$ K with 3366 water molecules. The simulation was

TABLE 4: Partial Charges for the SDS Molecule[a]

type *i*	*q*, eV
Na^+	+1.000
OM	−0.654
S	+1.284
OS	−0.459
CH2 (next to OS)	+0.137
CH2 (in the tail)	0.000
CH3	0.000

[a] The charges were adopted from ref 65.

run for 100 ns, of which 1 ns was regarded as a relaxation period because this provided ample time for the single SDS molecule to reach equilibrium with the water environment. Simulation data, including radial distribution functions and gauche defect probabilities, will be reported below in Section 3.

In the next step, self-aggregation and micellization were studied by varying the temperature and concentration of SDS molecules. The effect of temperature was studied in a system of 200 SDS molecules and 7902 water molecules (1 M concentration). Initially, the SDS molecules were placed uniformly randomly within the simulation box with the sodium counterions close to the head groups (see Figure 1). After this, the simulation box was filled with water, and the energy was minimized using the steepest descent algorithm. The same random initial configuration was used for all 200 ns MD simulations at eight different temperatures ranging from 253 to 323 K at 10 K intervals. The first 30 ns of the trajectories was considered as the initial micelle formation period and not included in the analysis. The remaining 170 ns was used for analysis. Specifically, although initial agglomeration takes place during the first 5 ns (see Figure 5), the micelle structure still evolves. Careful inspection of the micelle structural characteristics reveals that they have stabilized by 30 ns (data not shown). We also made an attempt to investigate the effect of concentration and system size on micellization. Although we were able to vary the concentration within a reasonable range, increasing the system size, proved to be computationally too intensive.

2.3. Data Analysis. Since the micelle-forming systems studied here have typically multiple micelles, we need to identify the micelles to which each SDS molecule belongs. We have adopted the following classification scheme based on geometrical considerations: The distance between the centers of mass, the distance between the C_5-atoms, and the distance between the C_{12}-atoms of the tails (see Figure 1) are computed for all pairs of SDS molecules. Any two SDS molecules are classified to be part of the same micelle if (1) one of these three distances is shorter than $R1_{cut} = 0.45$ nm, (2) two out of three distances are shorter than $R2_{cut} = 0.50$ nm, or (3) all three distances are shorter than $R3_{cut} = 0.60$ nm. These cutoffs where chosen after careful experimentation and visualization of the configurations to ensure accurate labeling. Figure 2 illustrates how the classification scheme works. It is noteworthy that employing these three different reference points allows us to distinguish the compound structure between (a) an ordered spherical micelle (typically C_{12} or center-of-mass-contact), (b) a disordered micelle (typically center-of-mass, or C_5-contact),

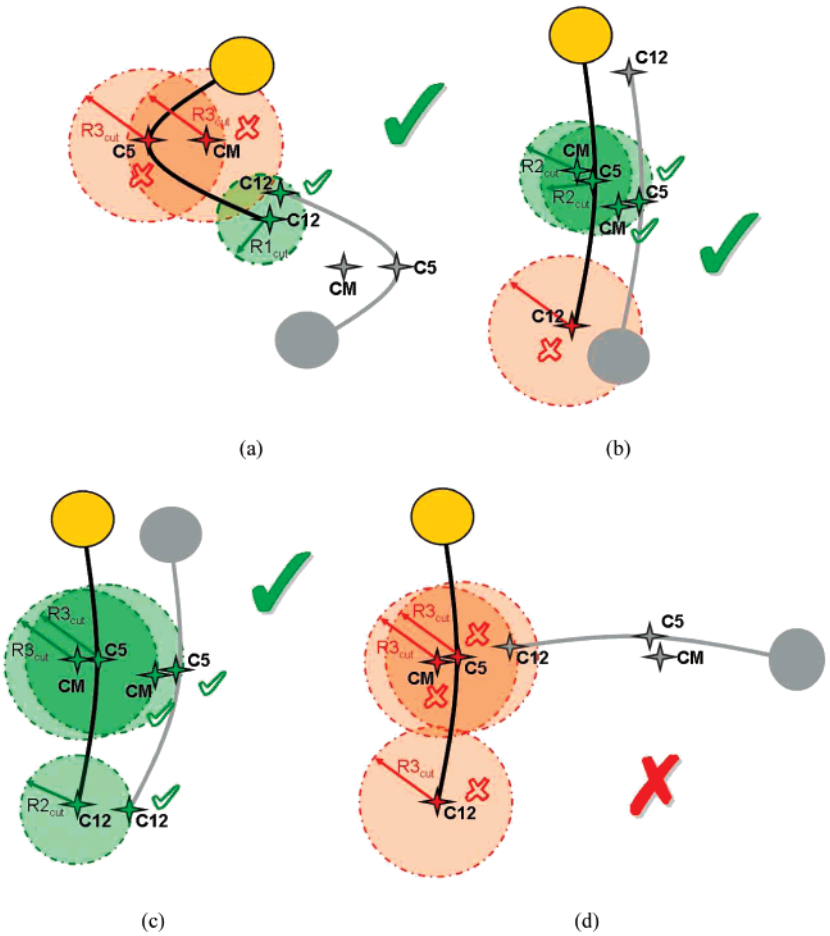

Figure 2. The micelle classification scheme. Two SDS molecules are classified to be in the same micelle if the C_5 atoms, the C_{12} atoms, or the centers of mass (CM) are within $R1_{cut}$ of each other (a), if any two pairs of these are within $R2_{cut}$ of each other (b), or if all three pair distances are are less than $R3_{cut}$ (c). (d) An example of a configuration in which the SDS molecules would not be classified as being in the same aggregate.

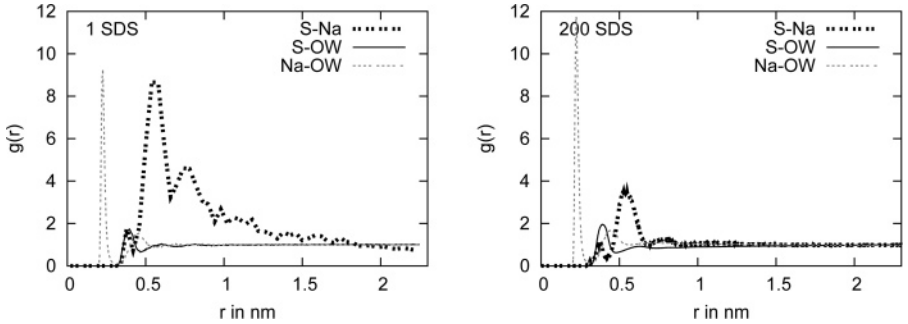

Figure 3. Radial distribution functions of 1 SDS molecule and 200 SDS molecules in water. In the legend, S is the head group sulfur atom, Na is the sodium counterion, and OW refers to the oxygen atom in a water molecule. The S−Na curve of the 1 SDS system appears less smooth than the others because the averaging is done over two individual atoms instead of over all the atoms of the particular type in the system.

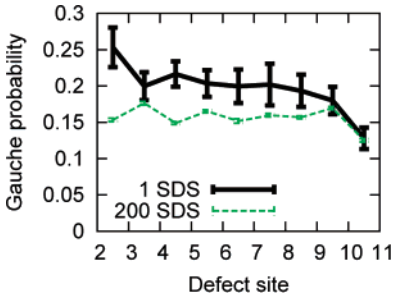

Figure 4. Gauche defect probability at $T = 323$ K for the hydrocarbon tail in systems of one SDS and 200 SDS molecules. As before, the data of the dilute limit has more fluctuations, thus resulting in a larger error estimate than in the 200 SDS micellized system.

or (c) an interdigiting crystal (typically C_5 or center-of-mass-contact). Of course, a given micelle may satisfy any combination of the above criteria and is classified as one unit.

Although the micelle classification scheme works very well for relatively large clusters (∼25 and larger), it does not catch all smaller micelles. To further improve the scheme, the clusters containing less than 25 SDS molecules were submitted to an additional check with the cutoffs increased by 25 %. This additional inspection removes the sensitivity in the classification scheme related to both shape fluctuations and the positions of individual SDS molecules in the micelles.

Where applicable, the error has been estimated as the standard deviation of the data sample.

3. Results

3.1. Dilute vs Concentrated Surfactant Solutions: Radial Distribution Functions and Hydrocarbon Tail Conformations. It is interesting to compare and contrast the behavior of the SDS molecules in terms of spatial correlations and hydrocarbon tail conformations in the dilute and concentrated limits. The dilute limit was achieved by inserting a single SDS molecule in an aqueous solution at $T = 323$ K and following its dynamics over 100 ns. Also note that the temperature $T = 323$ K is significantly above the micellization temperature of SDS, which has been reported to be 297 [4] or 288.7 K in the absence of NaCl[45] and 298 K in 0.6 M NaCl solution.[45] The concentration limit (1 M) was investigated by simulating the dynamics of 200 SDS molecules at the same temperature over 200 ns.

Figure 3 presents the radial distribution functions (RDF) that characterize the head group (sulfur)−sodium, head group (sulfur)−water, and sodium−water behavior. The latter two distribution functions behave in a very similar way, showing a sharp peak at 0.25 nm (0.4 nm) for sodium−water (sulfur−water) in both systems. On the other hand, the sulfur−sodium radial distribution function displays dramatic differences. In the concentrated 1 M solution in which SDS micellization takes place, the most visible change is the rapid leveling off of the RDF beyond the main binding peak; contrast this with the dilute case in which the RDF displays prominent peaks beyond the main binding peak, indicating long-range headgroup−sodium interactions. Nevertheless, both systems share the weak first binding shell (peak at ∼0.4 nm) and the main sodium binding peak beyond 0.5 nm.

The conformations of the SDS molecule can be characterized by the dihedral angle distribution and the resulting gauche defect density, that is, the probability of the hydrocarbon tail's having a kink. Here, a hydrocarbon sequence $i-j-k-l$ is defined to have a kink if the angle between the planes $i-j-k$ and $j-k-l$ is between 30 and 110 degrees. The gauche defect probability is presented in Figure 4 for both the 1 and 200 SDS systems at the same temperature, $T = 323$ K. It is noteworthy that the gauche defect probability per bond is higher for the individual SDS molecule. In the micellized system, the gauche probability is approximately equal for all sites in the hydrocarbon tail, but an isolated SDS has a higher kink probability toward the head group. Interestingly, the defect probability for the tail end of the molecule is the same in both systems, implying that micellization affects mostly the behavior of regions near the head group.

3.2. Temperature and Micelle Structure. We performed 200 ns simulations of 1 M SDS solution with 200 SDS molecules over a wide temperature range significantly below and above the critical micellization temperature (CMT), which has been reported to be 288.7,[45] 287.51,[46] or 297 K[4] on the basis of measurements at concentrations in the vicinity of CMC. In the simulations, the initial SDS aggregation takes place very rapidly, within the first few nanoseconds of the simulation. Figure 5 presents the aggregation numbers of the clusters as a function of time. We have considered the initial 30 ns for the initial micelle formation period and performed the analysis of system properties on the remainder of the trajectory. We stress that the analyzed trajectory most likely represents a sequence of metastable states; that is, the trajectories show indications that the system is still slowly evolving. Unfortunately, because of computational limitations, at the moment, it is infeasible to carry out simulations in which the system has sufficient time to equilibrate starting from a random initial configuration. Nevertheless, we believe that our results are important in elucidating the dynamics during the approach of the system toward equilibrium.

Let us next discuss the effects of temperature on micelle structure. Below the CMT, the predominant structure is a

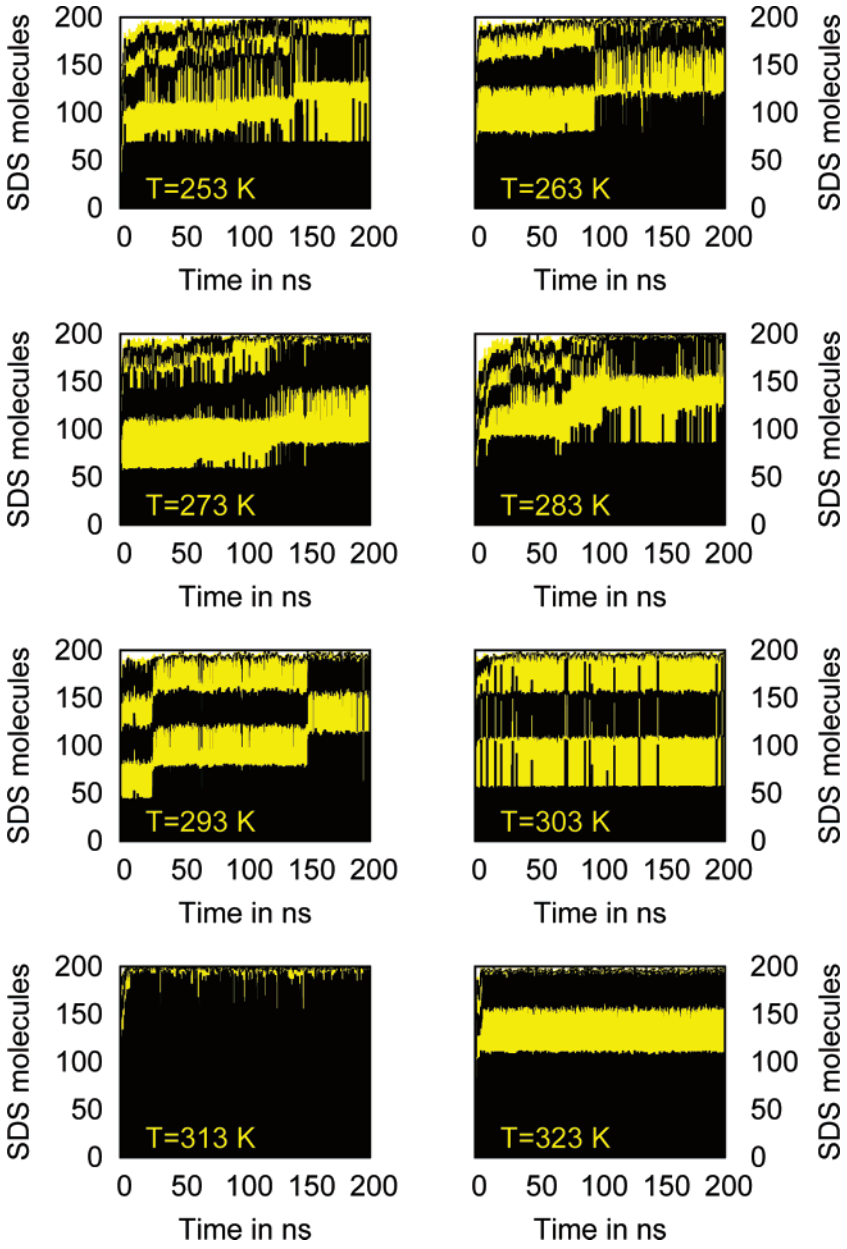

Figure 5. Micelle size distribution as a function of time. The X-axis presents the time in ns; the stripes show how the largest micelles evolve in size. The number of stripes tells the number of micelles present. The largest micelle is represented by the lowermost stripe at each analysis step. The width of the second stripe represents the size of the second largest micelle at each analysis step. Therefore, a disappearance of a stripe at any given time represents a fusion of two micelles. A temporary abrupt jump indicates that two aggregates were momentarily classified as one. This can happen, for example, if two micelles are very close to one another. On the other hand a crystalline cluster can be classified as two if the crystal has a stacking defect. For example, the $T = 313$ K system has from ~5 ns onward a slightly disorganized micelle of ~120 SDS molecules (see Figure 6). Because of the "fuzziness'' of this micelle, the smaller clusters occasionally are classified as being part of the larger aggregate, causing a momentary increase in size in the graphs. For micelle classification algorithm, see Section 2.3.

crystalline aggregate in which the SDS molecules settle aligned to a high degree either parallel or to form an interdigiting aggregate (see Figure 6a). This structure has a high degree of local translational order and corresponds to a solid crystalline phase. The final configuration at $T = 253$ K shows a system-spanning crystal, but the majority of crystalline aggregates are small because of the finite system size and the submicrosecond time period we were able to examine.

As the temperature is increased to $T = 273$ K, the first micelle emerges. However, most of the SDS molecules in our system still form crystalline aggregates at this temperature. At $T = 283$ and 293 K, the structural transition becomes more evident with the degree of crystallization decreasing. An isolated crystalline aggregate is still visible in the final configurations of $T = 303$ and 313 K, but these temperatures produce predominantly micellar configurations, whereas the aggregates formed at $T = 323$ K are entirely micellar. Examples of the crystalline and micellar aggregates are shown in Figure 6.

3.3. Systematic Assessment of Finite Size Effects. To assess possible finite size effects and possible artifacts due to periodic boundary conditions, we performed simulations of 200 and 400 SDS molecules at a fixed 700 mM concentration and compared sizes and shapes of the resulting aggregates. Figure 7 shows the micelle size development for the different system sizes. Due to the increased system size, the duration of the 400 SDS simulation is limited to 140 ns. The micelles are structurally identical in the two systems, at least within the studied time window. Both systems produce the largest micelle of size 60−

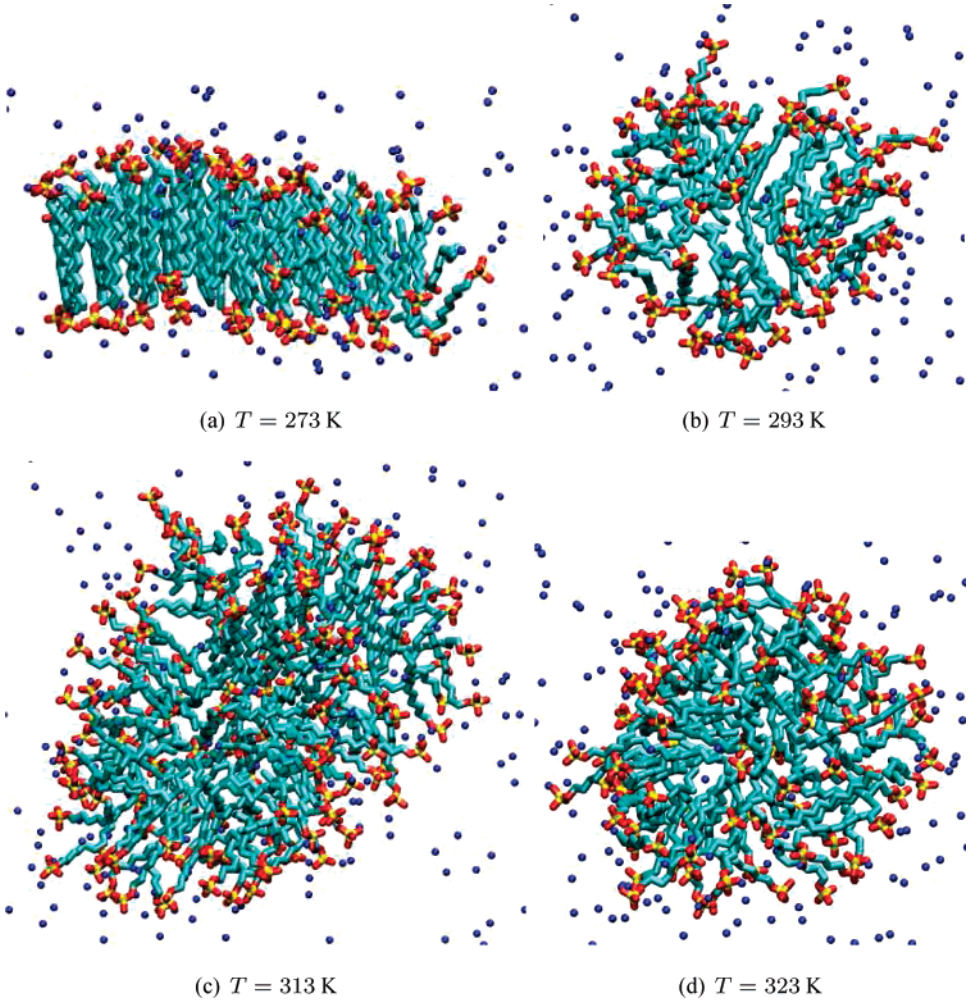

Figure 6. Examples of aggregate structures after 200 ns. Part a presents a crystalline aggregate ($T = 273$ K); part b, a spherical micellar aggregate ($T = 293$K). Parts c and d show a larger, elongated micelle structure ($T = 313$ K) and the $T = 323$ K final configuration, which is a micelle that is structurally between the 293 K and 313 K largest micelles; that is, slightly elongated. The difference in size between the micelles in parts b and d shows how the micellization process depends on thermodynamic fluctuations: by chance, the system at $T = 313$ K has taken a path that has resulted in a larger micelle than the $T = 323$ K system. The blue spheres represent sodium atoms, and surrounding micelles and water molecules have been omitted to facilitate visualization of the micelle. The snapshots correspond to the largest micelle in the system.

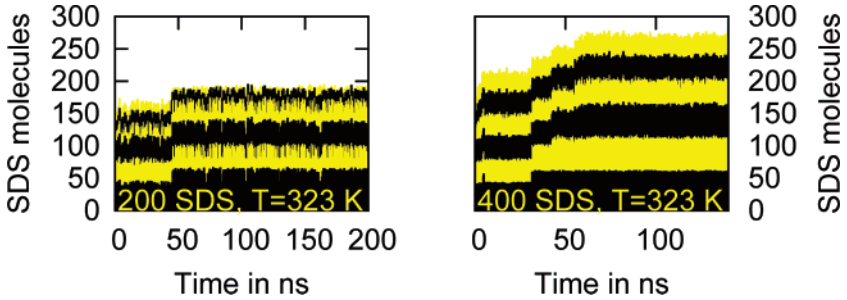

Figure 7. Micelle size distribution as a function of time for two different system sizes. Both systems have 700 mM concentration but differ in the number of SDS molecules (200, left; 400, right). The cumulative size of the six largest micelles is plotted in the graphs. This means that the bottom-most stripe represents the size of the largest micelle, the width of the second stripe corresponds to the size of the second largest micelle, and so on, thus providing a plot in which the total column height is the cumulative size of the six largest micelles. See also Figure 5 for more details about how to read this plot. Note the difference in the duration of the simulations.

70 SDS molecules, but the graphs show indications that the micelle size could be evolving toward a larger aggregate. Determining whether that is the case would require microsecond simulations, and that is beyond current capabilities. Because the forming micelles in the two systems are equivalent, we conclude that our choice of limiting the system size to 200 SDS molecules is reasonable.

3.4. Surfactant Concentration and Micelle Structure. It is well-known that for ionic surfactant, the mean micelle size is a function of surfactant concentration at elevated molarities. It is interesting to study the effect of the overall surfactant concentration on micelle formation kinetics and structure. To this end, we have systematically varied the concentration from the relatively high 1 M concentration discussed in Section 3.2. More specifically, we have performed simulations also on two larger systems of 200 SDS molecules, corresponding to 700 and 200 mM concentrations, respectively, and compared these to the 1 M system. Whereas the 1 M 200 SDS system contains

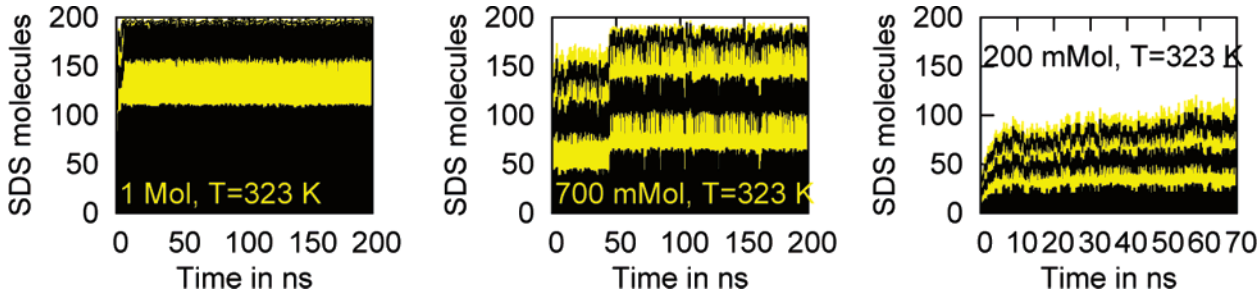

Figure 8. Micelle size distribution as a function of time in concentration varying between 1 M and 200 mM. All systems have 200 SDS molecules, but the concentration varies between 1 M, 700 mM, and 200 mM. The cumulative sizes of the six largest micelles are plotted in the graphs. This means that the bottom-most stripe represents the size of the largest micelle, the width of the second stripe corresponds to the size of the second largest micelle, and so on, thus providing a plot in which the total column height is the cumulative size of the six largest micelles. See also Figure 5 for more details about how to read this plot.

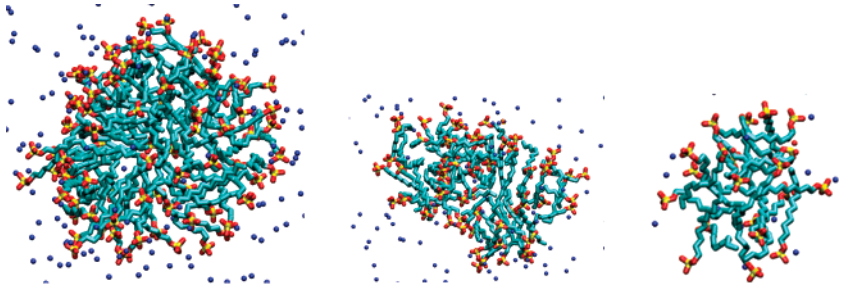

Figure 9. Micellization as a function of concentration. The largest micelle in systems of 200 SDS molecules in a concentration of 1 M (a), 700 mM (b), and 200 mM (c) is visualized. The temperature is 323 K. The micelles correspond to the final configurations of the simulations; that is, 200 (1 M), 200 (700 mM), and 70 ns (200 mM).

7902 water molecules and periodic bondary conditions, the 700 mM system contains 13 395, and the 200 mM system, 49 905 water molecules, respectively.

It is evident from the simulation data for the micelle size distribution, shown in Figure 8, that the micelle formation kinetics is significantly faster at elevated concentrations. The 1 M system is stable in micelle size for the duration of the simulation (200 ns), whereas the 700 mM system has significantly more fluctuations and is still evolving at the end of the simulation (200 ns). Similarly, the 200 mM system shows a clear increasing trend in micelle size during the whole simulation period (70 ns). The data shown in Figure 8 supports the conclusion that our model would produce a smaller micelle size at decreasing concentration, in agreement with experiments. However, we are unable to draw a definite conclusion due to the fact that the larger systems, especially the 200 mM system, have clearly not yet stabilized in micelle size. Unfortunately, computational resources limit the practical extent of the simulations.

The effects of concentration from the structural point of view are displayed in Figure 9, where we plot the largest micelles of the final configurations of the simulations. The essential difference comes from the micelle size: The largest micelle in the 1 M system is slightly deformed toward an elliptical form, whereas the micelles with size between 40 and 80 SDS molecules are approximately spherical, although deformed micelles, such as the largest micelle in the 700 mM system at 200 ns (see Figure 9b) also exist. The aggregates in the 200 mM system appear significantly less spherical. This is due to the fact that the micellization process is still underway; the aggregates are very small at this point, but they are still growing, as Figure 8 indicates.

We conclude that the high SDS concentration used in this work is likely to affect the micelle size in our simulations. However, with the exception of minor ellipsoidal deformation at higher concentration, the micelle structure appears to remain similar. We emphasize that because of computational limitations, even the lowest concentration we examined, that is, 200 mM, is still significantly above the CMC. Thus, extrapolation of our results to concentrations near CMC is not straightforward.

3.5. Micelle Structural Analysis. To characterize the micelle structure further, we analyzed the trajectories of the 1 M 200 SDS systems from 30 ns onward. The probability distribution of finding C1, C6, C12, S, or Na atoms as a function of distance from the center of mass of the largest micelle in the system is presented in Figure 10. The graphs reflect the effects of the structural change from crystal fragments to micelles. At the two lowest temperatures, that is, at $T = 253$ and 263 K, the configurations are purely crystalline. This shows as the curves of C1, C6, and C12 coinciding to a large extent. At $T = 253$ K, the probability of finding C6 close to the center of mass is larger than that of finding C12 or C1. This is a direct consequence of the interdigiting structure of the crystal fragments (see Figure 6). As a result of the emergence of the micellar structure, the graphs from $T = 273$ K onward present clear peaks in Na, S, C1, and C6. These peaks shift according to the size of the aggregate, that is, $T = 273$, 293, and 303 K have the C1 and S peaks at approximately 1.6−1.7 nm. On the other hand, at $T =$ 283, 313, and 323 K, the peaks occur beyond 2 nm, reflecting the presence of a larger aggregate.

The peaks corresponding to $T = 283$ and 313 K are compact and unimodal, with the exception of the Na curve of $T =$ 283 K. In contrast to this, most peaks in the graphs corresponding to temperatures at 273 K and above have traces of bimodal or even more complex form. This a result of the dynamics of the system: The "largest micelle" may change during the analysis period, and the graphs presented here are time averages over the entire analysis period. This is most visible in the graphs

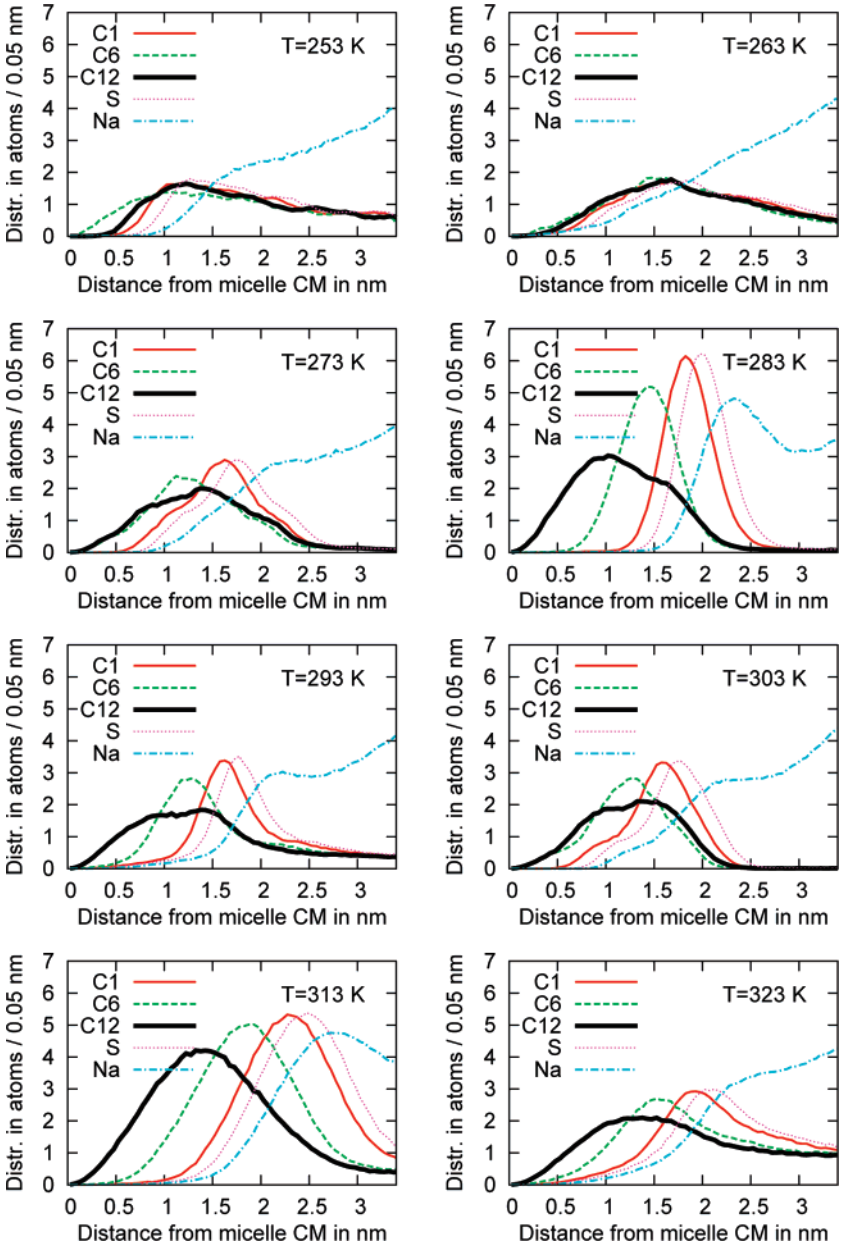

Figure 10. Distribution of C1, C6, C12, S, and Na atoms measured from the CM of the largest micelle in the system. The plotted quantity is the number of atoms of the particular type in a shell of width 0.5 Å.

for $T = 273$ and 303 K, which correspond to systems that have formed two aggregates of almost equal size (see Figure 5). Furthermore, since one of the aggregates is micellar in structure and the other is a crystalline fragment, we observe an average of graphs corresponding to both structures.

The Na curves of Figure 10 corresponding to micellar aggregates display a prominent peak at the outer shell of the micelle. This results from the counterion aggregation close to micelles, which results in regions more dilute in counterions. The dilute regions correspond either to cores of other micelles in the system (which are void of counterions) or to bulk water regions, which contain a much smaller average density of counterions than regions in close proximity to the micelle. On the other hand, the monotonically increasing Na curves at lower temperatures corresponding to crystalline aggregates indicate that the counterions are more evenly distributed in the system. This results from the large size of the main aggregate and the fact that it has a V-shaped form for a part of the simulation at $T = 263$ K. Since the center of mass of this largest crystalline aggregate when V-shaped is close to water, the probability distribution at $T = 263$ K appears more uniform than, for example, the $T = 253$ K curve.

With regard to temperature effects on the hydrocarbon tail conformations, the gauche probability of each bond (as shown in Figure 11) increases as a function of temperature, implying that the molecules become more rigid and elongated at low temperatures, as expected. Increasing temperature correlates very strongly with an elevated probability of gauche defects. The structural transition from rigid interdigiting crystals to flexible sphere-forming molecules can also be observed in the plot: $T = 253$ K and $T = 263$ K have very low gauche defect probabilities, whereas the curves corresponding to $T = 273$ and 283 K show a significantly higher defect probability. Dominantly micellar systems at $T = 293-313$ K form another cluster in the gauche defect graph, and the all-micellar $T = 323$ K system has ~16% probability per site for the tail to be kinked. Interestingly, Figure 11 shows an increased probability for observing gauche defects toward the head group end, as well

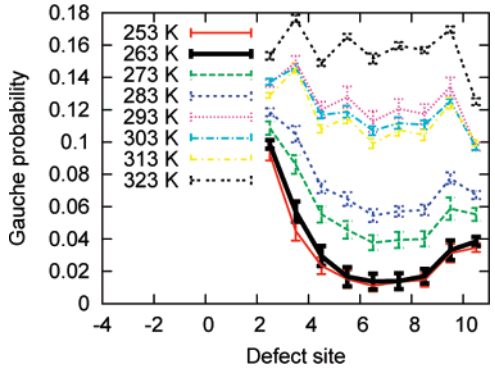

Figure 11. Gauche defect probability for different sites in the tail of the SDS molecule. The carbon site numbering starts from the C atom next to the SO_4 head group and is plotted so that, for example, 2.5 refers to the bond between second and third carbon atom in the tail. Nonpolar hydrogen atoms are treated as a compound with the neighboring carbon atom, and therefore, the horizontal axis ranges bonds from 2.5 to 10.5.

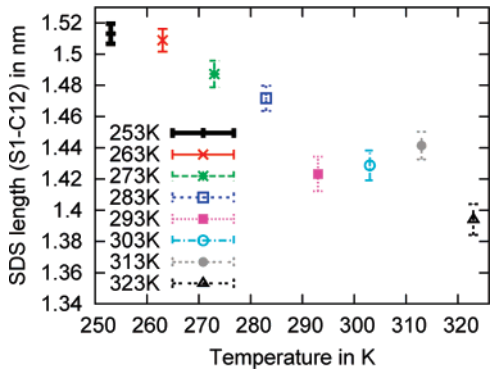

Figure 12. SDS length as a function of temperature. The length is reported as the average S−C12 distance with standard deviation as the estimate of error.

as a smaller increase toward the tail end in the curves corresponding to the predominantly crystalline phase. The latter results from the crystalline structure: if the SDS molecule is not perfectly at level with the rest of the SDS molecules in the crystal due to fluctuations (especially near the crystal edges), it is energetically favorable for the ends of the molecule to kink to maximize the number of hydrophobic neighbors. This is reflected in the increased defect probability in the head and end regions of the tail. On the other hand, the micellar structures formed at higher temperatures are much less ordered, and hence, the curves corresponding to dominantly micellar structure level out with even a slight defect probability decrease at the tail end.

Another quantity closely related to the frequency of gauche defects in the SDS molecules is their average length, defined as the linear separation between the sulfur atom and the C12 atom in the tail. The data shown in Figure 12 are in line with the gauche defect data: the graph shows a clear trend in the average length as a function of temperature. At low temperatures, the molecules are elongated in the crystalline aggregates, whereas at elevated temperatures in the micellar regime, they "shorten'' by ~10%. Interestingly, the effect of temperature becomes weaker as most of the surfactants become incorporated within micelles. At intermediate temperatures, the average length is strongly temperature-dependent as more and more surfactants prefer micellar structures over the crystalline aggregates.

Counterion binding is an essential quantity in assessing the structure of ionic micelles. In particular, interactions of counterions with the charged head groups may lead to formation of

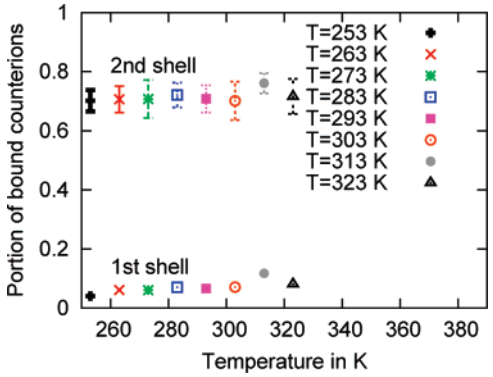

Figure 13. Counterion binding as a function of temperature. The upper set of symbols corresponds to counterions within $D = 0.675$ nm (second shell) from a head group sulfur atom, and the lower set, to a portion of counterions within $D = 0.425$ nm (first shell).

long-lived clusters and ionic bridges, adding to the stability of the system.[47] We assess the sodium counterion binding by calculating the fraction of sodium atoms within a predetermined cutoff of any head group sulfur atom. The cutoffs are obtained from the corresponding RDF (see Figure 3): the count is stopped at either 4.25 Å, which corresponds to the first peak in the radial distribution function, or at the second peak at $r = 6.75$ Å. The results are presented in Figure 13. The key feature in this data is that the sodium−micelle head group interaction is mainly through the second shell. Put differently, only a very small fraction of sodium ions reside within the first integration shell. Interestingly, the binding appears to be quite insensitive with regard to temperature within the studied temperature range. The sodium ions do not migrate into the interior of the micelles.

Finally, the radial distribution functions of S−OW (as shown in Figure 3) imply that the first hydration shell of the head group has a radius of 0.5 nm as measured from the sulfur atom. No dependence of the RDF on temperature was observed. On the basis of this data, we calculate the hydration number of the head group and obtain a value of eight water molecules, again independent of temperature.

4. Discussion

We have investigated the formation of micellar aggregates using large-scale MD simulations. First, we have provided a parametrization for SDS within Gromacs (available on-line at www.softsimu.org). Then, by employing this parametrization, we focused on a system of 200 SDS and 7902 water molecules at varying temperatures both below and above the CMT. The longest simulations reported in this paper were run over 200 ns. Additionally, we simulated an isolated SDS molecule in bulk water to verify the model and larger systems having more water and up to 400 SDS molecules. The latter simulations were used to assess possible finite size artifacts and the dependence of micelle aggregation on surfactant concentration. Although the behavior of the 200 SDS versus 400 SDS system in 700 mM concentration does not indicate strong finite size effects, surfactant concentration was found to have a strong effect of both micelle structures and formation kinetics in the 200 SDS 200, 700, and 1000 mM systems in which the concentration was varied.

In the simulations, we observe a structural transition from crystalline interdigitating aggregates to micellar structures with increasing temperature. This transition took place between 273 and 313 K in the simulations, but the strong dominance of micellar aggregates at $T = 303$ and 313 K leads us to believe that in our model, the transition temperature is most likely below

303 K. The rather wide coexistence region of the crystalline and micellar phases is most likely due to long-lived (≫200ns) metastable states above the thermodynamic transition temperature. Nevertheless, our results are consistent with the reported CMTs for SDS: 288.7,[45] 287.51,[46] or 297,[4] depending on measurement at concentrations close to the CMC = 8 mM ± 1.4 mM, again depending on measurement.[48−53] The CMT has also been reported to increase with salt or SDS concentration.[45,46]

The systems that form crystalline or partially crystalline aggregates, that is, $T < 313$ K, quite swiftly form clusters that have a size in the range of 50−70 SDS molecules (see Figure 5, $T = 253-303$ K). The aggregate size is stable for the duration of the simulation (200 ns). At $T = 313$ and 323 K, the aggregate size is significantly larger, more than 100 SDS molecules. This difference can be traced to the change in the aggregate structure: for the crystalline (interdigitating) phase, the equilibrium state corresponds to a macroscopic crystal, whereas the micellar phase has a concentration-dependent equilibrium aggregation number. In the temperature region corresponding to crystalline aggregates, we observe apparently stabilized crystal clusters instead of a system-wide macroscopic crystal because of the submicrosecond time window and the small system size in the simulations. A similar phenomenon takes place in the coexistence region: once formed, the crystal fragments and spherical micelles are relatively stable. However, in the $T =$ 313 and 323 K systems, apparently, thermal fluctuations are large enough to fuse the smaller micelles to form the larger aggregates that are observed.

The equilibrium micelle size (i.e., aggregation number) of SDS close to the CMC has been reported to be 55−77 molecules.[50,53−55] Furthermore, it is well-known that the aggregation number of ionic micelles grows as a function of concentration.[54,56−59] Within the range of concentrations we have studied, the micelle size should be larger than the micelles observed at $T = 313$ and 323 K and potentially rod-shaped.[54,59] However, the swollen micelles present at high SDS concentrations have been reported to be polydisperse in size, which indicates a rather small free energy difference between the aggregate sizes.[5,60] We are, however, restricted by the simulation description: Once formed, the micelles are in a local energy minimum, and if the minimum is deep enough, it is unlikely that we see further size evolution within the submicrosecond time window we are able to examine. We conclude that observed micelle sizes provide a lower limit to the actual micelle sizes in the experiments.

We have assessed our model against the experimentally observed increase in SDS micelle size as a function of concentration[54,56−59] by varying it between 1 M and 200 mM. Although the conclusions are preliminary, especially in the more dilute limit, due to limited computational resources, we observe indications that the systems at lower concentration are heading toward smaller equilibrium micelle sizes than the more concentrated 1 M system. After 200 ns, the 700 mM system at $T = 323$ K provides micelles of 50−70 SDS molecules, whereas the micelles observed at 200 mM concentration are half the size. However, both systems are still slowly evolving, and the data are not sufficient to provide conclusions on what the final model-predicted equilibrium micelle size in each concentration is. On the basis of experiments, we would expect the micelle size at 200 mM concentration to be ∼100 SDS molecules.[54,59] However, as we have mentioned before, the micelle sizes we observe provide a lower limit to the micelle size in the experiments.

With regard to the micellar structure, the head group sulfur atoms were mostly located at distances between 1.8 and 2.0 nm from the micelle center (as shown in Figure 10) in the systems corresponding to aggregation number below 70. In micelles larger than this, the peak shifts beyond 2 nm. The values are in excellent agreement with experimental values; that is, 1.89 nm[61] for lithium dodecyl sulfate, 1.673 nm for the hydrophobic core radius of SDS micelle,[53] and theoretical predictions of 1.970 ± 0.008 nm[22] for the SDS micelle radius. In agreement with our observations, Yoshii et al.[62] predict the shift in the peak position with the increase in the size of the SDS micelle. However, they also predict that the growth of aggregation number promotes an empty core for the resulting elongated micelles. In our simulations, the C12 distribution near the micelle center is very similar, regardless of the micelle size (see Figure 10). The reason for this is most likely the fact that we start from a random initial configuration, and the duration of the simulations is 200 ns instead of the 1.5−4.5 ns of ref 62. Furthermore, ref 63 presents a very similar trend in the increase of the micelle radius from 1.72 to ∼ 2.3 nm with an increasing excess NaCl concentration from 0 to 0.35 M.

The observed structural variety and the difference in aggregate sizes complicate the overall comparison of the density distributions reported here to those of previous work. In Figure 10, the $T = 283$ K graph corresponds to a system in which the largest micelle is throughout the analysis period approximately spherical and only slightly larger than, for example, in ref 22, in which the micelle has a fixed size of 60 SDS molecules. Thereby, the graph is well in agreement with the ones reported in refs 20 and 22, as well as with the density distribution graph calculated for an interfacial monolayer in ref 64. The other graphs of Figure 10 contain contributions of crystalline or larger micellar aggregates, thus altering the probability distributions accordingly.

The gauche defect probability was observed to depend mainly on the aggregate structure and, hence, on temperature (see Figure 11). At $T = 323$ K, the defect probability is ∼16% per site, whereas the crystalline aggregates at $T = 253$ and 263 K have kinks only with probability of 0.02% in the center regions of the tail and up to 10% near the head group. Reference 65 reports gauche defect probabilities of 24 or 28% for the SDS tail, depending on the environment, whereas ref 64 reports gauche defect probabilities on the order of 20−30% in the bulk tail and as high as 45% near the end at $T = 300$ K. It is noteworthy that the data come from simulations with different force fields for systems in which the SDS molecules form a monolayer.

Let us briefly discuss the relatively wide range of temperatures employed in this study (253−323 K). In our approach, we have employed the same force field parametrization at all temperatures, and it is natural to ask whether the model can accurately capture the main features of aggregation away from the ambient temperature, where the fitting was originally done. To the best of our knowledge, systematic studies of temperature-dependent quantities are few. An example of such is the recent transport coefficient study of Baştuğ and Kuyucak.[66] They demonstrated that self-diffusion coefficients of water and several ions are reasonably well described in a temperature range 300−323 K. These results are encouraging in the sense that the dynamics of the system is captured over a relative wide range of temperatures. In a more complicated system of glycolipids in which hydrogen-bonding plays a major role, Róg et al.[67] have shown that close to a thermodynamic phase transition, the force field description may have to be modified. Here, we do not have such a problem because our system is much simpler and not dominated by hydrogen bonding. As a final example, Lyubartsev et al.[68] have shown in the context of coarse graining

that the potentials remain robust, even under varying salt concentration, and reproduce correct diffusion and viscous properties. Although we are unable to carry out a detailed comparison of, for example, the gauche defect probability against experiments due to the lack of appropriate experimental data, we predict a strong temperature dependence, which should be amenable to experimental verification.

In our simulations, the counterions mainly reside close to the aggregate surface. Our observation that counterion binding takes place to a large part through the second shell is in agreement with observations of MacKerell.[22] However, the simulational studies of Yoshii and Okazaki[69] and Rakitin and Pack[27] report a majority of the counterions binding through the first shell, and Bruce et al.[70] reported 25% sodium binding through the first shell and 50% through first and second shell in their simulations. In contrast, we observe only 5−10% of the counterions bound through the first shell and ∼70% of the counterions bound through the first or the second shell. We suspect that this discrepancy results from differences in the simulation models or from the much shorter, at most 5 ns long,[70] simulation times combined with the predetermined micelle form used in refs 27, 69, and 70. Our observation that approximately 70% of the counterions are bound through the first or the second shell is a value exactly in line with the values of the counterion binding parameter β reported as $\beta = 0.72$ in ref 71 and counterion dissociation parameter α, which has been reported as 0.29,[72] 0.26 ± 0.02,[46] 0.272 ± 0.017,[73] 0.371,[53] or 0.36 ± 0.02,[74] depending on the method.

With regard to the hydration number of the SDS head group, it was observed to be 8 with no observable temperature or aggregate structure dependency. The hydration number is in excellent agreement with the results of Bales et al.,[58] who obtained the best fit to experimental polarity index with a hydration number of 9. Although Bales et al.[58] also report a decrease in the hydration number as the average micelle size increases, we observe no such trend. It should be emphasized that the specific hydration number 8 we obtained is calculated as an average over all the 200 SDS molecules in the system. Our hydration number thus includes contributions from various aggregate sizes, which may mask any potential aggregate size dependent phenomena.

To summarize, the computational model employed here is able to reproduce experimental results of SDS micelle structure, ionization degree, and hydration. On the other hand, predicted defect probabilities in the hydrocarbon chain differ somewhat from prior computational predictions; we presume that this is due to different computational models employed in the past and varying micelle sizes observed in the simulations. Furthermore, due to the limited time scale in the simulations, we are unable to make definite predictions for micelle size and critical micellization temperature.

5. Conclusions

We have performed extensive molecular dynamics simulations of SDS in explicit solvent. After introducing a novel parametrization of SDS within Gromacs, we focused on obtaining more insight into the micellization process and the structure of micellar aggregates as a function of temperature and surfactant concentration. As discussed in detail above, the model reproduces experimental and prior theoretical results to a very high accuracy. Our simulations provide a window into the complex aggregation kinetics during micellar self-assembly, and we hope to report on even more extensive simulations in the future.

Acknowledgment. This work has been supported by Academy of Finland (M.S.), Emil Aaltonen foundation (M.K.), the Natural Sciences and Engineering Council of Canada (M.K.), and through an NSF-DMR Grant No. 0449184 (M.H.). We also thank the Southern Ontario SharcNet (www.sharcnet.ca) grid computing facility for computer resources.

References and Notes

(1) Philip, D.; Stoddart, J. F. Self-assembly in natural and unnatural systems. *Angew. Chem., Int. Ed.* **1996**, *35*, 1155−1196.

(2) Whitesides, G. M.; Grzybowski, B. Self-assembly at all scales. *Science* **2002**, *295*, 2418−2421.

(3) Percec, V.; Ungar, G.; Peterca, M. Self-assembly in action. *Science* **2006**, *313*, 55−56.

(4) Helenius, A.; Simons, K. Solubilization of membranes by detergents. *Biochim. Biophys. Acta* **1975**, *415*, 29−79.

(5) Zana, R. *Dynamics of Surfactant Self-Assemblies: Micelles, Microemulsions, Vesicles and Lyotropic Phases*; CRC Press: Boca Raton, FL, 2005; Vol. 126.

(6) Fredrickson, G. H.; Bates, F. S. Dynamics of block copolymers: Theory and experiment. *Ann. Rev. Mater. Sci.* **1996**, *26*, 510−550.

(7) Chernik, G. G. Phase studies of surfactant−water systems. *Curr. Opin. Colloid Interf. Sci.* **1999**, *4*, 381−390.

(8) Torchilin, V. P.; Lukyanov, A. N.; Gao, Z.; Papahadjopoulos-Sternberg, B. Immunomicelles: Targeted pharmaceutical carriers for poorly soluble drugs. *Proc. Natl. Acad. Sci.* **2003**, *100*, 6039−6044.

(9) Yong, W.; Lomakin, A.; Kirkitadze, M. D.; Teplow, D. B.; Chen, S.-H.; Benedek, G. B. Structure determination of micelle-like intermediates in amyloid β-protein fibril assembly by using small angle neutron scattering. *Proc. Natl. Acad. Sci.* **2001**, *99*, 150−154.

(10) Shelley, J. C.; Shelley, M. Y. Computer simulation of surfactant solutions. *Curr. Opin. Colloid Interface Sci.* **2000**, *5*, 101.

(11) Larson, R. G. Self-assembly of surfactant liquid crystalline phases by Monte Carlo simulation. *J. Chem. Phys.* **1989**, *91*, 2479−2488.

(12) Larson, R. G. Monte Carlo simulation of microstructural transitions in surfactant systems. *J. Chem. Phys.* **1992**, *96*, 7904−7918.

(13) Dill, K. A.; Kopper, D. E.; Cantor, R. S.; Dill, J. D.; Bendedouch, D.; Chen, S.-H. Molecular conformations in surfactant micelles. *Nature* **1984**, *309*, 42−46.

(14) Dill, K. A.; Flory, P. J. Molecular organization in micelles and vesicles. *Proc. Natl. Acad. Sci.* **1981**, *78*, 676−680.

(15) Dill, K. A. Configurations of the amphiphilic molecules in micelles. *J. Phys. Chem.* **1982**, *86*, 1498−1500.

(16) Drouffe, J.-M.; Maggs, A. C.; Leibler, S. Computer simulations of self-assembled membranes. *Science* **1991**, *254*, 1353, Nov.

(17) Bast, T.; Hentschke, R. Molecular dynamics simulation of a micellar system. *J. Mol. Model.* **1996**, *2*, 330−340.

(18) Goetz, R.; Lipowsky, R. Computer simulations of bilayer membranes: self-assembly and interfacial tension. *J. Chem. Phys.* **1998**, *108*, 7397−7409.

(19) Bandyopadhyay, S.; Klein, M. L.; Martyna, G. J.; Tarek, M. Molecular dynamics studies of the hexagonal mesophase of sodium dodecylsulphate in aqueous solution. *Mol. Phys.* **1998**, *95*, 377−384.

(20) Gao, J.; Ge, W.; Hu, G.; Li, J. From homogeneous dispersion to micelles−a molecular dynamics simulation on the compromise of the hydrophilic effects of sodium dodecyl sulfate in aqueous solution. *Langmuir* **2005**, *21*, 5223−5229.

(21) Cheong, D. W.; Panagiotopoulos, A. Z. Monte Carlo simulations of micellization in model ionic surfactants: Application to sodium dodecyl sulfate. *Langmuir* **2006**, *22*, 4076−4083.

(22) Madkerell, A. D., Jr. Molecular dynamics simulation analysis of a sodium dodecyl sulfate micelle in aqueous solution: Decreased fluidity of the micelle hydrocarbon interior. *J. Phys. Chem.* **1995**, *99*, 1846−1855.

(23) Tieleman, D. P.; van der Spoel, D.; Berendsen, H. J. C. Molecular dynamics simulations of dodecylphosphocholine micelles at three different aggregate sizes: Micellar structure and chain relaxation. *J. Phys. Chem. B* **2000**, *104*, 6380−6388.

(24) Marrink, S. J.; Tieleman, D. P.; Mark, A. E. Molecular dynamics simulation of the kinetics of spontaneous micelle formation. *J. Phys. Chem. B* **2000**, *104*, 12165−12173.

(25) Bruce, C. D.; Senapati, S.; Berkowitz, M. L.; Perera, L.; Forbes, M. D. E. Molecular dynamics simulations of sodium dodecyl sulfate micelle in water: The behavior of water. *J. Phys. Chem. B* **2002**, *106*, 10902−10907.

(26) Yamamoto, S.; Maruyama, Y.; aki Hyodo, S. Dissipative particle dynamics study of spontaneous vesicle formation of amphiphilic molecules. *J. Chem. Phys.* **2002**, *116*, 5842−5849.

(27) Rakitin, A. R.; Pack, G. R. Molecular dynamics simulations of ionic interactions with dodecyl sulfate micelles. *J. Phys. Chem. B* **2004**, *108*, 2712−2716.

(28) Lazaridis, T.; Mallik, B.; Chen, Y. Implicit solvent simulations of dpc micelle formation. *J. Phys. Chem. B* **2005**, *109*, 15098−15106.

(29) Woods, M. C.; Haile, J. M.; O'Connell, J. P. Internal structure of a model micelle via computer simulation. 2. spherically confined aggregates with mobile head groups. *J. Phys. Chem.* **1986**, *90*, 1875−1885.

(30) Stephenson, B. C.; Beers, K.; Blankschtein, D. Complementary use of simulations and molecular-thermodynamic theory to model micellization. *Langmuir* **2006**, *22*, 1500−1513.

(31) Berendsen, H. J. C.; van der Spoel, D.; van Drunen, R. Gromacs: A message-passing parallel molecular dynamics implementation. *Comp. Phys. Comm.* **1995**, *91*, 43−56.

(32) Lindahl, E.; Hess, B.; van der Spoel, D. 3.0: a package for molecular simulation and trajectory analysis. *J. Mol. Model.* **2001**, *7*, 306−317.

(33) van der Spoel, D.; Lindahl, E.; Hess, B.; Groenhof, G.; Mark, A. E.; Berendsen, H. J. C. Gromacs: Fast, flexible, and free. *J. Comp. Chem.* **2005**, *26*, 1701−1718.

(34) Berendsen, H. J. C.; Postma, J. P. M.; van Gunsteren, W. F.; DiNola, A.; Haak, J. R. Molecular dynamics with coupling to an external bath. *J. Chem. Phys.* **1984**, *81*, 3684−3690.

(35) Hess, B.; Bekker, H.; Berendsen, H. J. C.; Fraaije, J. G. E. M.: A linear constraint solver for molecular simulations. *J. Comp. Chem.* **1997**, *18*, 1463−1472.

(36) Miyamoto, S.; Kollman, P. A. Settle: an analytical version of the shake and rattle algorithms for rigid water models. *J. Comp. Chem.* **1992**, *13*, 952−962.

(37) Essman, U.; Perela, L.; Berkowitz, M. L.; T. Darden, H. L.; Pedersen, L. G. A smooth particle mesh Ewald method. *J. Chem. Phys.* **1995**, *103*, 8577−8592.

(38) York, D. M.; Darden, T. A.; Pedersen, L. G. The effect of long-range electrostatic interactions in simulations of macromolecular crystals: A comparison of the and truncated list methods. *J. Chem. Phys.* **1993**, *99*, 8345−8348.

(39) Patra, M.; Karttunen, M.; Hyvönen, M. T.; Lindqvist, P.; Falck, E.; Vattulainen, I. Molecular dynamics simulations of lipid bilayers: Major artifacts due to truncating electrostatic interaction. *Biophys. J.* **2003**, *84*, 3636−3645.

(40) Patra, M.; Karttunen, M.; Hyvönen, M. T.; Falck, E.; Vattulainen, I. Lipid bilayers driven to a wrong lane in molecular dynamics simulations by truncation of long-range electrostatic interactions. *J. Phys. Chem. B* **2004**, *108*, 4485−4494.

(41) van Gunsteren, W. F.; Berendsen, H. J. C. *Gromos-87 manual*. Biomos BV, Nijenborgh 4, 9747 AG Groningen, The Netherlands, (1987).

(42) Patra, M.; Karttunen, M. Systematic comparison of force fields for microscopic simulations of NaCl in aqueous solutions: Diffusion, free energy of hydration and structural properties. *J. Comput. Chem.* **2004**, *25*, 678−689.

(43) Berendsen, H. J. C.; Postma, J. P. M.; van Gunsteren, W. F.; Hermans, J. Interaction models for water in relation to protein hydration. In Intermolecular Forces; Pullman, B., Ed., 1981; Reidel: Dordrecht, The Netherlands; pp 331−342.

(44) Humphrey, W.; Dalke, A.; Schulten, K. Visual Molecular Dynamics. *J. Mol. Graphics* **1996**, *14*, 33−38.

(45) Mazer, N. A.; Benedek, G. B.; Carey, M. C. An investigation of the micellar phase of sodium dodecyl sulfate in aqueous sodium chloride solutions using quasielectric light scattering spectroscopy. *J. Phys. Chem.* **1976**, *80*, 1075−1085.

(46) Vautier-Giongo, C.; Bales, B. L. Estimate of ionization degree of ionic micelles based on Krafft temperature measurements. *J. Phys. Chem. B* **2003**, *107*, 5398−5403.

(47) Zhao, W.; Róg, T.; Gurtovenko, A. A.; Vattulainen, I.; Karttunen, M. Atomic-scale structure and electrostatics of anionic POPG lipid bilayers with Na^+ counterions. *Biophys. J.* **2006**, *92*, 1114−1124.

(48) Esposito, C.; Colicchio, P.; Facchiano, A.; Ragone, R. Effect of weak electrolyte of the critical micellar concentration of sodium dodecyl sulfate. *J. Colloid Interface Sci.* **1998**, *200*, 310−312.

(49) Gu, G.; Yan, H.; Chen, W.; Wang, W. Observation of micelle formation and micellar structural transition from sphere to rod by micro-calorimetry. *J. Colloid Interface Sci.* **1996**, *178*, 614−619.

(50) Johnson, I.; Olofson, G.; Jönsson, B. Micelle formation of ionic amphiphiles. *J. Chem. Soc. Faraday Trans. 1* **1987**, *83*, 3331.

(51) Joshi, T.; Mata, J.; Bahadur, P. Micellization and interaction of anioinic and nonionic mixed surfactant systems in water. *Colloids Surf. A* **2005**, *260*, 209−215.

(52) Cifuentes, A.; Bernal, J.; Diez-Masa, J. C. Determination of critical micellization concentration values using capillary electrophoresis instrumentation. *Anal. Chem.* **1997**, *69*, 4271−4274.

(53) Bastiat, G.; Grassl, B.; Khoukh, A.; Francois, J. Study of sodium dodecyl sulfate−poly(propylene oxide) methacrylate mixed micelles. *Langmuir* **2004**, *20*, 5759−5769.

(54) Quina, F. H.; Nassar, P. M.; Bonilha, P. M.; Bales, B. L. Growth of sodium dodecyl sulfate micelles with detergent concentration. *J. Phys. Chem.* **1995**, *99*, 17028−17031.

(55) Hayter, J. P.; Penfold, J. Determination of micelle structure and charge by neutron small-angle scattering. *Colloid Polym. Sci.* **1983**, *261*, 1022−1030.

(56) Hall, D. G. Polydispersity of sodium dodecyl sulfate (SDS) micelles. *Langmuir* **1999**, *15*, 3483−3485.

(57) Croonen, Y.; Geladé, E.; van der Zegel, M.; van der Auweraer, M.; Vandendriessche, H.; de Scgryver, F. C.; Almgren, M. Influence of salt, detergent concentration, and temperature on the fluorescence quenching of 1-methylpyrene in sodium dodecyl sulfate with m-dicyanobenzene. *J. Phys. Chem.* **1983**, *87*, 1426.

(58) Bales, B. L.; Messina, L.; Vidal, A.; Peric, M.; Nascimiento, O. R. Precision relative aggregation number determination of SDS micelles using a spin probe. A model of micelle surface hydration. *J. Phys. Chem B* **1998**, *102*, 10347−10358.

(59) Griffiths, P. C.; Paul, A.; Heenan, R. K.; Penfold, J.; Ranganathan, R.; Bales, B. L. Role of counterion concentration in determining micelle aggregation: Evaluation of the combination of constraints from small-angle neutron scattering, electron paramagnetic resonance, and time-resolved fluorescence quenching. *J. Phys. Chem. B* **2004**, *108*, 3810−3816.

(60) Siemiarczuk, A.; Ware, W. R. A novel method for determining size distributions in polydisperse micelle systems based on the recovery of fluorescence lifetime distributions. *J. Phys. Chem.* **1993**, *97*, 8082−8091.

(61) Bendedouch, D.; Chen, S.-H.; Koehler, W. C. Structure of ionic micelles from small angle neutron scattering. *J. Phys. Chem.* **1983**, *29*, 441.

(62) Yoshii, N.; Okazaki, S. A molecular dynamics study of structural stability of spherical SDS micelle as a function of its size. *Chem. Phys. Lett.* **2006**, *425*, 58−61.

(63) Bockstahl, F.; Pachoud, E.; Duplatre, G.; Billard, I. Size of sodium dodecyl sulphate micelles in aqueous NaCl solutions as studied by positron annihilation spectroscopy. *Chem. Phys.* **2000**, *256*, 307−313.

(64) Domnguez, H. Computer simulations of surfactant mixtures at the liquid/liquid interface. *J. Phys. Chem. B* **2002**, *106*, 5915−5924.

(65) Schweighofer, K. J.; Essmann, U.; Berkowitz, M. Simulation of sodium dodecyl sulfate at the water−vapor and water−carbon tetrachloride interfaces at low surface coverage. *J. Phys. Chem. B* **1997**, *101*, 3793−3799.

(66) Bastug, T.; Kuyucak, S. Temperature dependence of the transport coefficients of ions from molecular dynamics simulations. *Chem. Phys. Lett.* **2005**, *408*, 84−88.

(67) Róg, T.; Vattulainen, I.; Karttunen, M. Modeling glycolipids: Take one. *Cell. Mol. Biol. Lett.* **2005**, *10*, 625−630.

(68) Lyubartsev, A. P.; Karttunen, M.; Vattulainen, I.; Laaksonen, A. On coarse-graining by the inverse Monte Carlo method: Dissipative particle dynamics simulations made to a precise tool in soft matter modeling. *Soft Mater.* **2002**, *1*, 121−137.

(69) Yoshii, N.; Okazaki, S. A molecular dynamics study of surface structure od spherical SDS micelles. *Chem. Phys. Lett.* **2006**, *426*, 66−70.

(70) Bruce, C. D.; Berkowitz, M. L.; Perera, L.; Forbes, M. D. E. Molecular dynamics simulations of sodium dodecyl sulfate micelle in water: Micellar structural characteristics and counterion distribution. *J. Phys. Chem. B* **2002**, *106*, 3788−3793.

(71) Shanks, P. C.; Franses, E. I. Estimation of micellization parameters of aqueous sodium dodecyl sulfate from conductivity data. *J. Phys. Chem.* **1992**, *96*, 1794−1805.

(72) Stigter, D.; Mysels, K. J. Tracer electrophoresis. ii. The mobility of the micelle of sodium lauryl sulfate and its interpretation in terms of zeta potential and charge. *J. Phys. Chem.* **1955**, *59*, 45−51.

(73) Bales, B. L. A definition of the degree of ionization of a micelle based on its aggregation number. *J. Phys. Chem. B* **2001**, *105*, 6798−6804.

(74) Aswal, V. K.; Goyal, P. S. Selective counterion condensation in ionic micellar solutions. *Phys. Rev. E: Stat. Phys., Plasmas, Fluids, Relat. Interdiscip. Top.* **2003**, *67*, 051401.